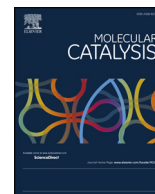




Contents lists available at ScienceDirect

Molecular Catalysis

journal homepage: www.elsevier.com/locate/mcat

Porous cobalt@N-doped carbon derived from chitosan for oxidative esterification of 5-Hydroxymethylfurfural: The roles of zinc in the synthetic and catalytic process

Yamei Lin^a, Guo-Ping Lu^{a,b}, Xin Zhao^b, Xun Cao^b, Lele Yang^a, Baojing Zhou^a, Qin Zhong^a, Zhong Chen^{b,*}

^a School of Chemical Engineering, Nanjing University of Science & Technology, Xiaolingwei 200, Nanjing 210094, China

^b School of Materials Science & Engineering, Nanyang Technological University, 50 Nanyang Avenue, Singapore 639798, Singapore

ARTICLE INFO

Keywords:

Cobalt nanoparticles
Zinc
Porous N-doped carbon
Chitosan
Oxidative esterification of hydroxymethylfurfural

ABSTRACT

A newly developed, facile and sustainable self-sacrifice template strategy, in which zinc and chitosan were used as the sacrificial template and carbon source respectively, has been disclosed for the synthesis of a hollow Co-embedded in nitrogen-doped graphite (Co@CN) structure. This material exhibits excellent catalytic efficiency in the oxidative esterification of 5-hydroxymethylfurfural to 2,5-furandicarboxylic acid dimethyl ester that is a significant raw material for polymer synthesis. According to the experimental and calculation results, zinc as the self-sacrificial template and acid-base site regulator has significantly improved the performance of the catalyst. The high specific surface area owing to the partial evaporation of zinc and the optimization of basic and acid sites in the catalyst prove to be the main reasons for its high activity.

Introduction

The utilization of biomass to produce valuable chemicals and materials has become a key point in the modern sustainable industry due to its renewability, safety and low cost [1–4]. Among the platform chemicals derived from biomass, 5-hydroxymethylfurfural (HMF) accessible from six-carbons sugars and their polymers, has been used to bridge the gap between lignocellulosic biomass and important biochemicals [2,5,6]. The oxidation of HMF to 2,5-furandicarboxylic acid (FDCA), one of the top-10 biobased products from biorefinery carbohydrates, is one of the most significant reaction steps for the conversion of HMF. FDCA can be used in the production of poly(ethylene-2,5-furandicarboxylate) (PEF) [7]. However, there is still a dearth of straightforward and ecofriendly methods for the purification of FDCA owing to its poor solubility and high boiling point [5]. The production of 2,5-furandicarboxylic acid dimethyl ester (FDMC) may eliminate the issue due to its good solubility. Moreover, FDMC can also be used directly to synthesize polymers through transesterification reaction [8].

Although a large number of attempts have been developed for the oxidation of HMF into FDCA, using methods such as homogeneous and heterogeneous catalysis, [9–15] electrocatalysis [16–18] and biocatalysis [19], only a few reports have mentioned the oxidative esterification of HMF. In general, this transformation is catalysed by noble metals

(Au, Pd) with the help of high pressure or excess bases [20–26]. A few earth-abundant-metal catalysts have also been explored, but high temperature and O₂ pressure are needed, and the selectivity is still poor in some cases (see more details in Table S1). [27–30] Meanwhile, most of the previous reports on HMF oxidation took place in dilute solutions (0.05–0.3 M) due to the highly reactive groups in HMF, which significantly hampers both FDMC production on an industrial scale. Furthermore, Co-embedded in nitrogen-doped graphite (Co@CN) prove to be an efficient catalyst for base-free oxidation of alcohols to esters [27,28,31]. Therefore, we envisage that a novel Co@CN might be suitable for the base-free oxidative esterification of HMF under mild conditions with higher concentration of the substrate.

Shell biorefinery, referring to the fractionation of crustacean shells into their major components and the transformation of these components into value-added chemicals and materials, has attracted growing attention in recent years [32–35]. One of these major compounds is chitosan with lots of amine groups, making its binding affinity for transition-metal ions higher than other biomass [36]. Thus, chitosan should be an ideal precursor for the generation of metal@N-doped carbon materials. More recently, several metal@N-doped carbon materials derived from chitosan and its derivatives have been developed for electrocatalysis [37,38], organic synthesis [39–43] and pollutant degradation [44]. Based on the low boil point of zinc, Jiang and his co-

* Corresponding authors at: School of Materials Science & Engineering, Nanyang Technological University, 50 Nanyang Avenue, Singapore 639798, Singapore.
E-mail addresses: glu@njust.edu.cn (G.-P. Lu), ASZChen@ntu.edu.sg (Z. Chen).

<https://doi.org/10.1016/j.mcat.2019.110695>

Received 22 August 2019; Received in revised form 17 October 2019; Accepted 20 October 2019

2468-8231/ © 2019 Elsevier B.V. All rights reserved.

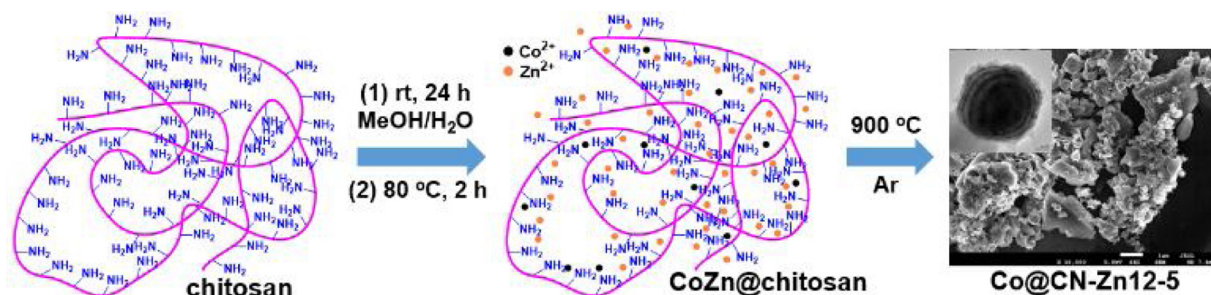


Fig. 1. The procedures for the preparation of Co@CN-Zn12-5.

workers have introduced a sacrificial template strategy for the synthesis of porous Co@CN from bimetallic Co-Zn ZIFs [45]. Along this line, we reasoned that both Co^{2+} and Zn^{2+} could coordinate with $-\text{NH}_2$ or $-\text{OH}$ groups of chitosan to form CoZn@chitosan, which can then be pyrolyzed at a temperature (e.g., $900\text{ }^\circ\text{C}$) to allow evaporation or partial evaporation of Zn to generate a porous Co@CN (illustrated in Fig. 1).

Ideally, the biomass conversion would be catalyzed by the materials based on biomass too. Herein, we demonstrate the first example on the synthesis of porous Co@CN derived from biomass for the oxidative esterification of HMF. Zinc plays crucial roles both in the synthetic and catalytic process. In the synthetic process, zinc as the self-sacrificed template can achieve the formation of porous Co@CN with high specific surface area (up to $658\text{ m}^2/\text{g}$). Moreover, the residual zinc in the catalyst can increase Lewis basic sites and decrease the strong Lewis acidic sites. These features may enhance the activation the O–H bonds [28] and αCH bonds of HMF [—46], and improve the interaction between catalyst and reactants [46].

Results and discussion

Initially, the amount of zinc salts and heating rate during the pyrolysis were investigated to optimize the catalytic activity of Co@CN using the oxidative esterification of HMF as the model reaction. The N_2 absorption/desorption isotherms and pore size distribution curves of various Co@CN-ZnX-Y (X for the weight ratio of Zn/Co, Y for the heating rate of pyrolysis) catalysts are shown in Figs. S1, S2 respectively. All of them are type IV patterns, which confirms these N-doped carbon materials have a mesoporous structure [41]. Notably, both

heating rate and the ratio of Zn/Co have significant influences on the BET surface areas, which affect the yield of FDMC (Fig. 2). In general, increasing the amount of zinc results in larger BET surface area due to the evaporation of Zn. More zinc remain in the material after pyrolysis when the ratio of Zn/Co increases to 16 which results in lower BET surface areas.

Meanwhile, a moderate heating rate is also necessary for guaranteeing the high BET surface area. The reasons may be explained that low heating rate keep the liquid Zn at a longer time which is harmful to form meso- or micro pores, and high heating rate may destroy the structure of the carbon material. Higher BET surface area can enhance the yield of FDMC owing to the improvement of the interaction between catalyst and reactant. Compared with other combinations, Co@CN-Zn12-5 (X = 15 and Y = 5) emerged as the optimum. Other cobalt catalysts including Co@AC (active carbon), CoZn@AC, Co@MgO, Co@ZrO₂ and Co@CeO₂ were employed as comparison, however the yields of FDMC were poor in all cases (Table S2).

The Raman spectra (Fig. S3) shows that both Co@CN-Zn0-5 and Co@CN-Zn12-5 have a considerable graphitization [47,48]. The graphitization of Co@CN-Zn0-5 is better than Co@CN-Zn12-5, which agrees with the powder XRD results (Fig. S4), and can explain that the decomposition temperature of Co@CN-Zn0-5 is higher than Co@CN-Zn12-5 (Fig. S5). The peaks at 44.2° and 51.5° can be seen in powder XRD patterns of Co@CN-ZnX-5 (X = 0, 4, 12) (Fig. S4), corresponding to the characteristic diffractions of (110), (200) lattice planes of metallic Co [47]. The surface morphology of Co@CN-ZnX-5 were also investigated by SEM (Fig. 3). As expected, the number of pores on the surface of catalysts are increased with increasing the Zn/Co ratio. This

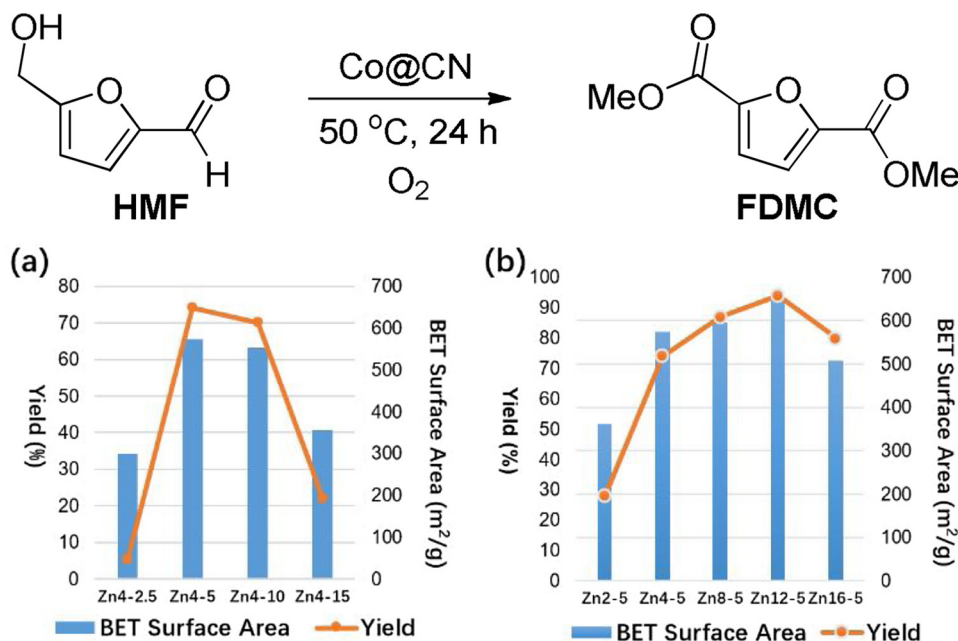


Fig. 2. The relationship between yields (yellow points) of FDMC (or BET surfaces areas (blue square)) with (a) The heating rate of pyrolysis; (b) the weight ratio of Zn/Co. Conditions: HMF 0.3 mmol, Co@CN 15 mol% of Co, MeOH 3 mL, O₂ 1 atm, $50\text{ }^\circ\text{C}$, 24 h; GC yields with nitrobenzene as an internal standard. (For interpretation of the references to colour in this figure legend, the reader is referred to the web version of this article).

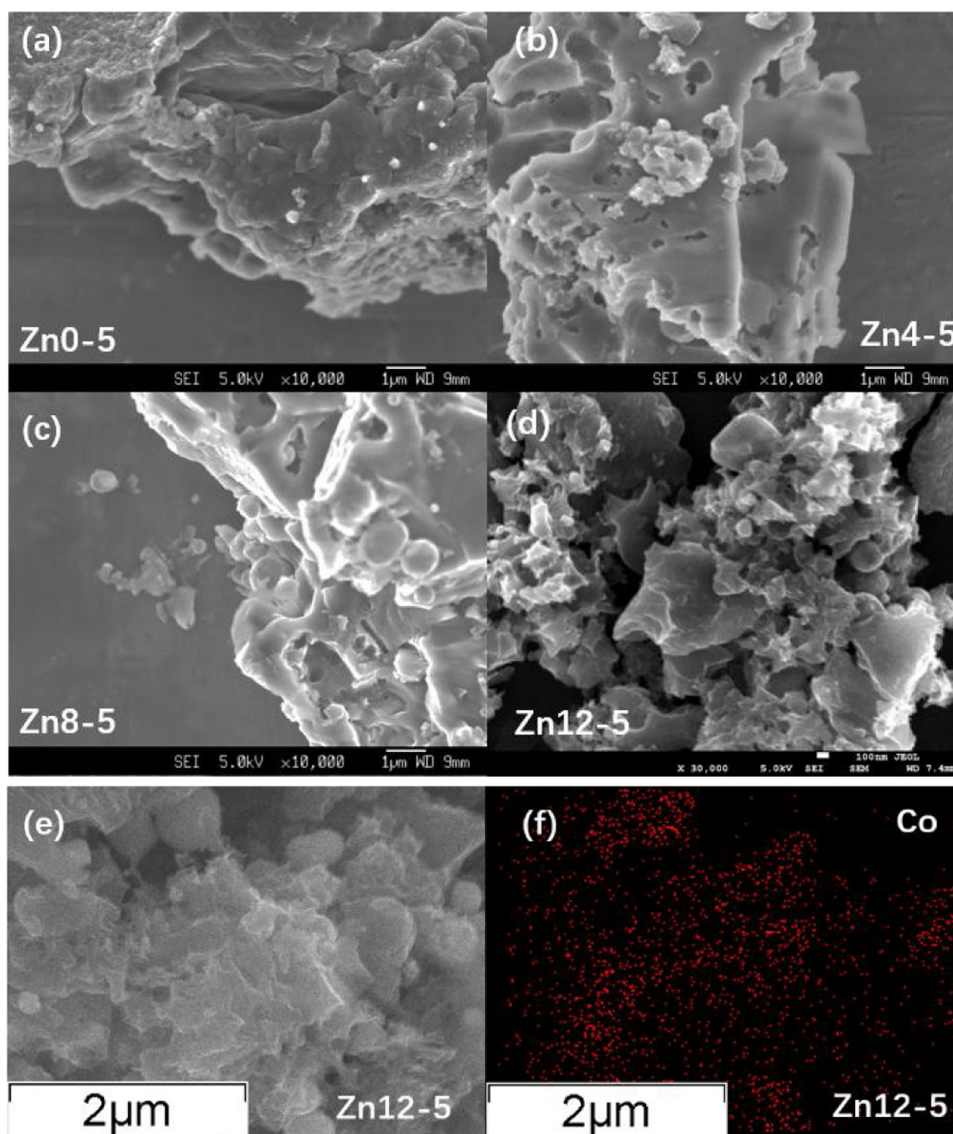


Fig. 3. SEM images of Co@CN-ZnX-Y. (a) Co@CN-Zn0-5; (b) Co@CN-Zn4-5; (c) Co@CN-Zn8-5; (d) Co@CN-Zn12-5; (e), (f) SEM mappings of Co@CN-Zn12-5.

observation from SEM is consistent with the BET results. Further SEM energy dispersive X-ray spectroscopy (EDS) mapping images of Co@CN-Zn12-5 indicate that most of metallic Co exists in the form of nanoparticles, and the rest is doped in the surface of carbon (Figs. 3e, 3f, 4a, 4b, S6).

As shown in Fig. 4, the Co nanoparticles are in the size range of 100–400 nm and load on the carbon material. The clear lattice fringes of 0.205 nm and 0.215 nm were observed from Co@CN-Zn12-5 corresponding to Co(111) and Co(100) respectively, [49] and the *d*-spacings of 0.250 nm is assigned to CoO(220) (Fig. 4d). [50] The HR-TEM image displayed in Fig. 4f shows two lattice fringes, corresponding to Co₃O₄(220). It should be noted that a small amount of zinc still exists in Co nanoparticles according to the TEM element mapping images (Fig. 5). ICP was used to measure the content of Co and Zn in Co@CN-ZnX-5 (Table S3). There are 0.05 wt% of Zn and 11.9 wt.% of Co in Co@CN-Zn4-5, while 1.27 wt.% of Zn and 11.7 wt.% of Co were detected in Co@CN-Zn12-5.

The chemical states of Co@CN-ZnX-5 (X = 0, 12) were further studied by XPS spectra (Fig. 6). Compared with Co@CN-Zn0-5, the Co peak of Co@CN-Zn12-5 shifts by 0.4 eV (779.1–779.5 eV) to the higher binding energy (Fig. 6a) owing to the presence of Co²⁺, Co³⁺ and Zn²⁺ (The peaks at 1021.3 and 1044.6 are assigned to Zn²⁺ in Fig. S7b) that

can reduce the electronic density of Co⁰ owing to inductive effects [49,51]. In addition, the peak intensity of Co 2p in Co@CN-Zn12-5 is much stronger than Co@CN-Zn0-5, proving that the evaporation of Zn during the synthetic process leads to more catalytic sites. The peaks at 397.7 eV and 400.3 eV belong to pyrrolic N (or Co-N_x) and pyridinic N respectively [40,47,48]. Both pyridinic N and Co-N_x could enhance the oxidation esterification of HMF by providing Lewis basic sites and catalytic sites [28].

In order to further determine the acid-base properties of Co@CN-ZnX-5, NH₃-temperature-programmed desorption (NH₃-TPD) and CO₂-TPD were tested (Fig. 7). In these catalysts, the Lewis acidic sites are corresponding to Co and Zn sites, and the Lewis basic sites are ascribing to N and O sites (CoO_x, CoN_x, pyridinic-N etc.). Co@CN-Zn12-5 has a similar amount of Lewis acidic sites with Co@CN-Zn4-5, and both of them have more acidic sites than Co@CN-Zn0-5 (Fig. 7c). Higher surface areas of Co@CN-Zn4-5 and Co@CN-Zn12-5 expose more Co and Zn sites, thus resulting more acidic sites. Co@CN-Zn12-5 have much more Lewis basic sites than the other two materials (Fig. 7d). Moreover, Co@CN-Zn4-5 has stronger acidic sites than Co@CN-Zn12-5 (Fig. 7c). It can be concluded that the presence of zinc in Co@CN-Zn12-5 increases the Lewis basic sites and decreases the Lewis acids sites [52,53].

To gain preliminary insights into the reaction mechanism, the

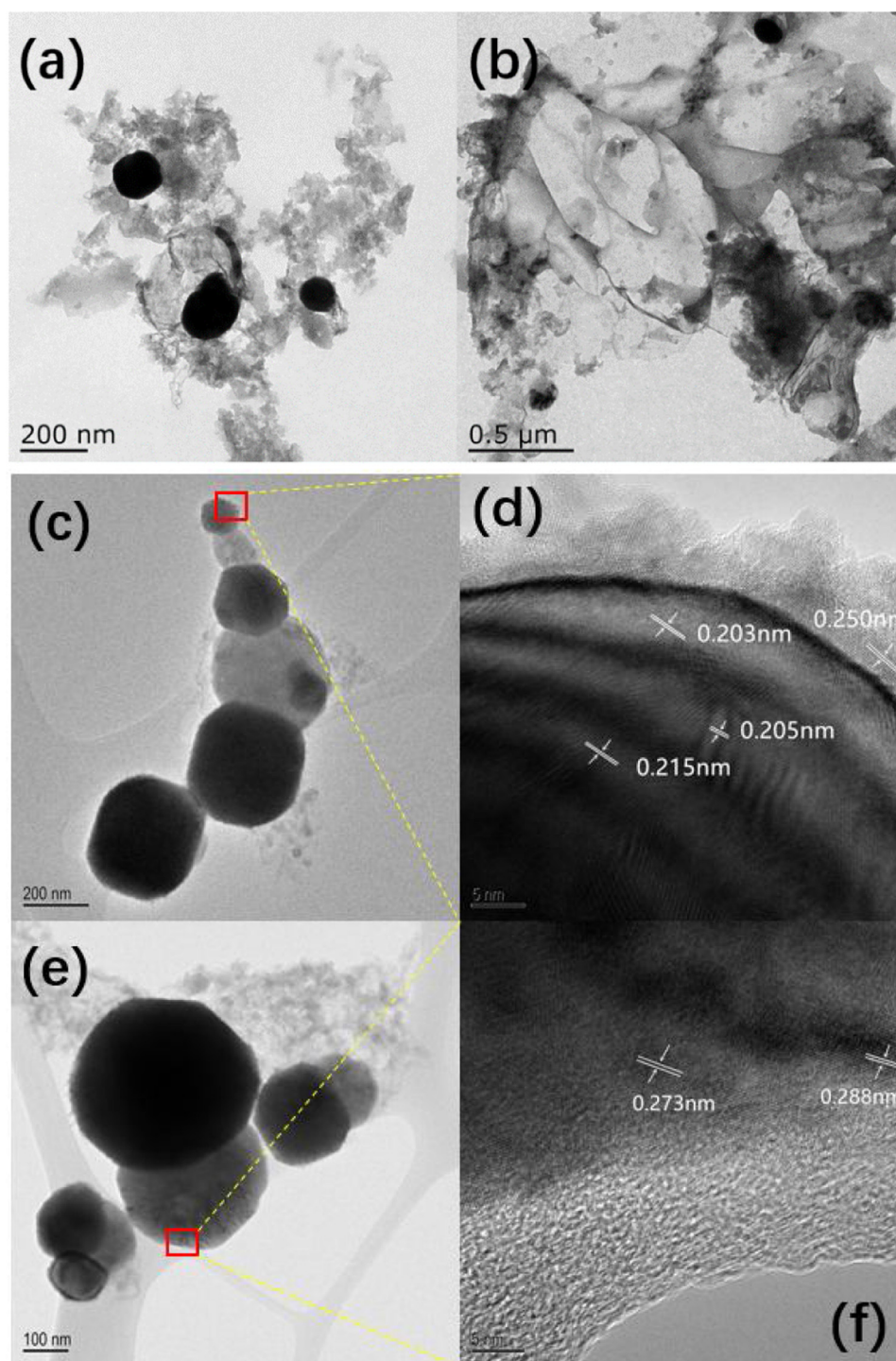


Fig. 4. (a), (b), (c), (e) TEM images of Co@CN-Zn5-12; (d), (f) HR-TEM images of Co@CN-Zn5-12.

oxidative esterification of HMF to FDMC was carried out using Co@CN-Zn12-5 as the catalyst tracked by GC and GC-MS. As shown in Fig. 8, HMF was gradually converted into FDMC with time. Compounds 2–4 generated when the reaction started, and all of them was consumed as the reaction proceeded. 4 had a higher yield than 2 and 3 at the beginning of the reaction. Based on these results and previous reports [30,54,55], a proposed oxidative esterification pathway of HMF to FDMC was illustrated in Scheme 1. It can be concluded that (1) 2, 3 and 4 are the intermediates of FDMC; (2) the major pathway is HMF-A-4-MFF-D-FDMC; (3) The step of 4 to MFF is the rate determination step. (4) The Lewis acid-base sites (AB) can enhance the hemiacetalization

(HMF to A, MFF to D). (5) The Co and Lewis basic sites (B) promote the oxidation of hemiacetal to the corresponding ester (A to 4, 4 to MFF, D to FDMC).

There is a thin layer of CoO_x on the surface of Co NPs based on TEM and XPS results, which may be the main catalytic sites of Co@CN-Zn12-5. Therefore, to further demonstrate the roles of residual zinc in the catalyst, the charge density maps of $\text{CoO-Zn}(110)$ and $\text{Co}_3\text{O}_4\text{-Zn}(110)$ were simulated based on density function theory (DFT). The results show that zinc has much lower charge density than cobalt (Fig. 9). This indicates that residual zinc can increase the charge density of CoO_x , which explains why zinc doping in the catalyst increases Lewis basic

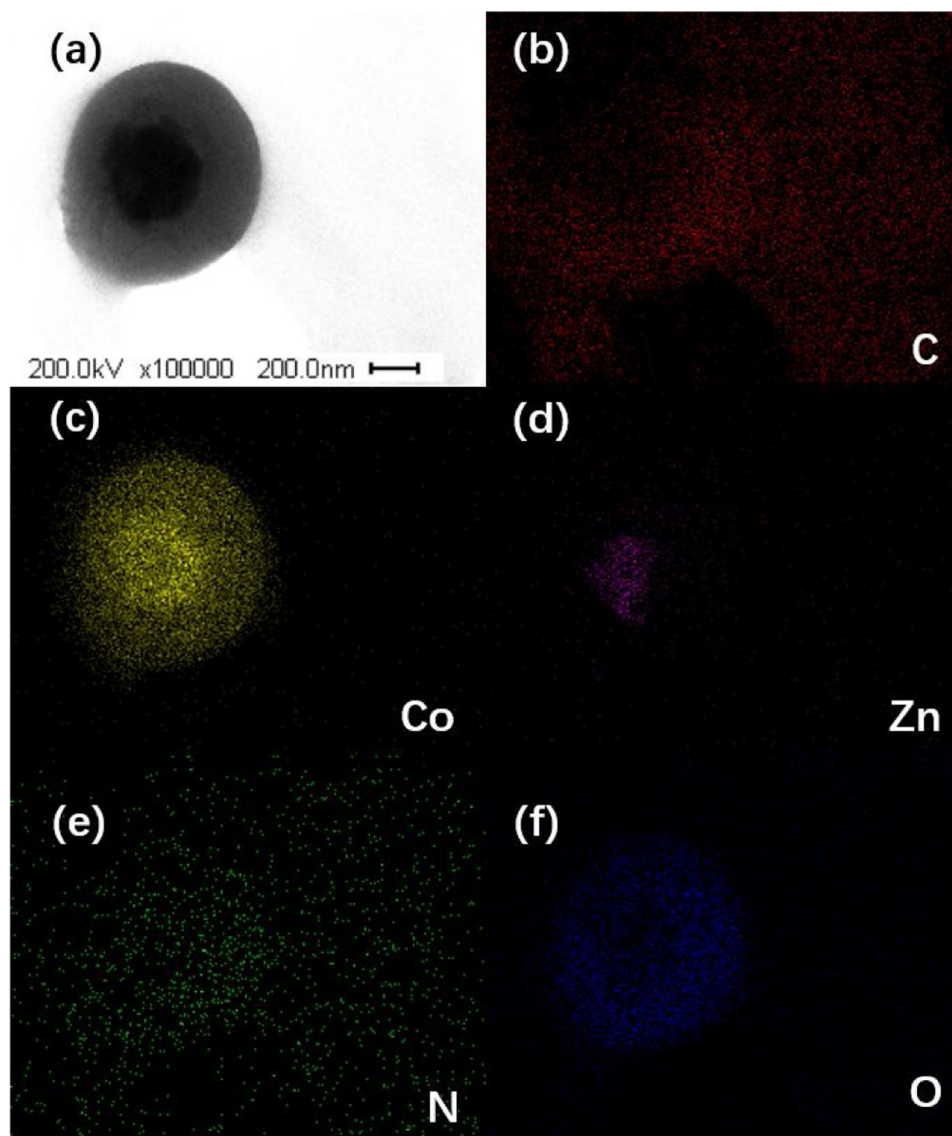


Fig. 5. TEM images and their corresponding element mapping images of Co@CN-Zn12-5.

sites and decreases the Lewis acids sites. The α -C-H dissociation of alcohol is the rate determination step in the oxidation (or oxidative esterification) of alcohol to carboxyl acid (or carboxyl ester) [54,55]. The Gibbs free energy profiles of the α -C-H dissociation suggest that CoO-Zn(110) has higher catalytic activity than CoO(110) (Table S4).

Based on the experimental and calculation results, there are several roles of zinc in the synthetic and catalytic process. (1) The evaporation

of zinc during the synthetic process results in the high specific surface area that increases the number of Lewis acidic sites; (2) the residual zinc in the catalyst leads to the increase of Lewis basic sites and decrease of the strong Lewis acidic sites; (3) the optimization of basic and acid sites not only improves the interaction between the catalyst and reactants (or intermediates, products), but also accelerates the deprotonation and α -CH dissociation processes [–38,45–47]. For example,

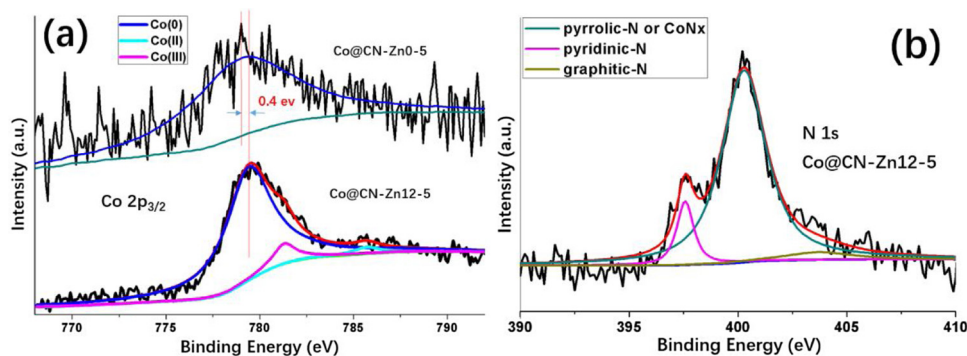


Fig. 6. XPS spectra: (a) Co $2p_{3/2}$ of Co@CN-ZnX-5 (X = 0, 12), (b) N 1s of Co@CN-Zn12-5.

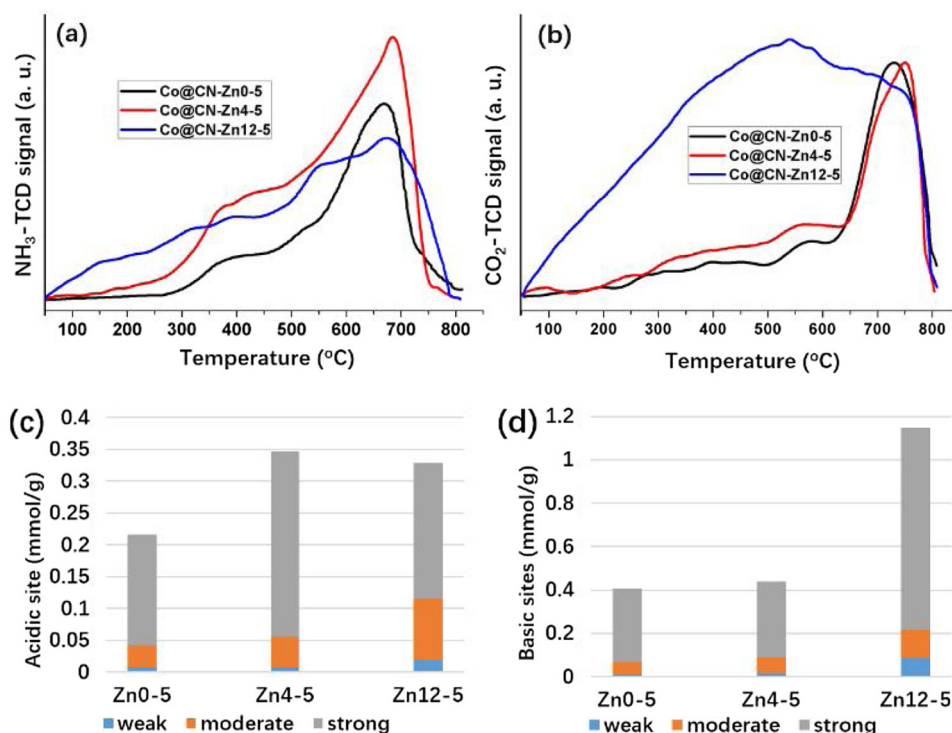


Fig. 7. (a) NH_3 -TPD profile, (b) CO_2 -TPD profile, the number of (c) acidic sites and (d) basic sites of Co@CN-ZnX-5 .

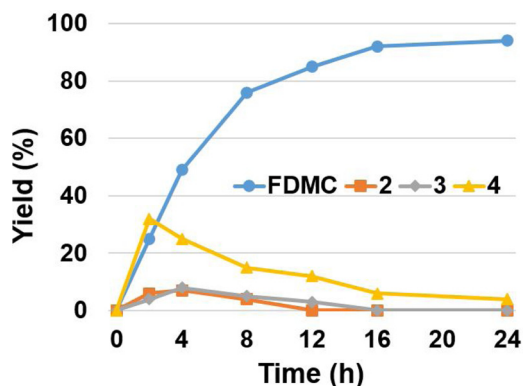


Fig. 8. Effect of reaction time on HMF conversion and selectivity of FDMC, 2, 3 and 4 over Co@CN-Zn12-5 (Reaction conditions: HMF 0.3 mmol, Co@CN 15 mol% of Co, MeOH 3 mL, O_2 1 atm, 50 °C, 24 h).

more Lewis basic sites enhances the deprotonation of alcohol, and more but weaker Lewis acidic sites (M of MN_x and MO_x , $\text{M} = \text{Co}, \text{Zn}$) promote the absorption of reactants and desorption of products.

The heterogeneous nature of the catalyst was demonstrated by a hot filtration experiment (Fig. 10). The catalyst was filtered off after 8 h at 50 °C, and the isolated solution was allowed to react for a further 16 h under identical conditions. No further increase in yield was observed. Studies were also conducted to assess the potential for recycling of the catalyst (Fig. 11). After completion of reaction, the catalyst was easily separated by centrifugation. Then it was washed with methanol to remove the absorbed organic chemicals, and dried in a vacuum oven at 60 °C. The crude product was further purified by flash column chromatography, and its structure was confirmed by NMR (Fig. S8). The results reveal that Co@CN-Zn12-5 could be reused at least four times in subsequent reactions without a significant loss of catalytic activity.

As shown in Fig. S9 the XRD spectra of recovery Co@CN-Zn12-5 indicate the same crystalline peaks with a reduced peak intensity after four runs. An obvious oxidation of the surface Co in the catalyst is found

based on XPS results (Fig. S7f). Meanwhile, an obvious aggregation of catalyst can be found in SEM images after four runs (Fig. S10), which is further confirmed by BET results (BET surface areas are reduced from 658 m^2/g to 494 m^2/g .) Moreover, ICP-MS analysis revealed a slight loss of the content of cobalt in Co@CN-Zn12-5 (Table S3, 11.7 wt.% to 10.9 wt.%) after recycling. The aggregation of catalyst and the oxidation of the surface Co may be the two main reason for the decrease in catalyst activity.

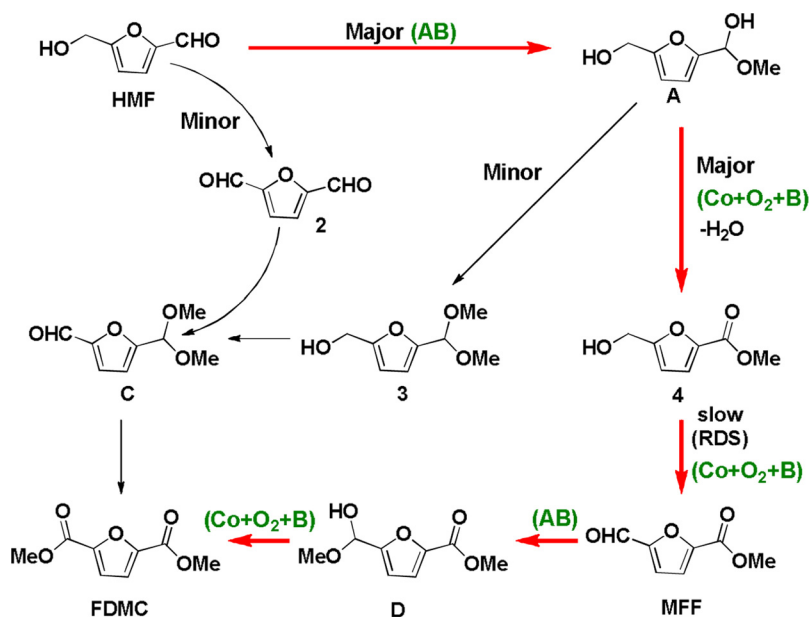
Conclusions

In summary, we have demonstrated a novel, efficient and sustainable sacrificial template method to synthesize a porous Co@CN catalyst that can utilize atmospheric oxygen for highly efficient base-free oxidative esterification of HMF under mild conditions (50 °C) at a high concentration (1 M) of the reactant. The evaporation of zinc during the synthetic process results in the high specific surface area with increased number of Lewis acidic sites, meanwhile the residual zinc in the catalyst leads to an increase of the Lewis basic sites and decrease of the strong Lewis acidic sites. Based on experimental and quantum calculation results, both features are beneficial to the catalytic activity of Co@CN-Zn12-5 owing to the improvement of the interaction between the catalyst and reactants (or intermediates, products) and the acceleration of the deprotonation and α -C-H dissociation processes. The dual roles of zinc during the synthetic and catalytic process provide a new idea for designing Porous transition-metal@CN. In addition, this strategy is easily scalable, so a more general applicability of such porous transition-metal@CN for other catalytic reactions are expected.

Experimental section

General

All chemicals were purchased from commercial suppliers and used directly without further purification. GC-MS was performed on an Waters Quattro micro™ GC that is a tandem quadrupole mass spectrometer equipped with Electron Impact (EI) and Chemical Ionization (CI



Scheme 1. Proposed oxidative esterification pathway of HMF to FDMC.

+/-CI-) sources. GC analyses are performed on an Agilent 7890A instrument (Column: Agilent 19091J-413: 30 m × 320 μm × 0.25 μm, carrier gas: H₂, FID detection). XRD analysis was performed on X-ray diffraction (XRD, Shimadzu 6000 X-ray diffractometer) with Cu Kα radiation (λ = 0.154 nm). High-resolution transmission electron microscopy (HR-TEM) and selected area electron diffraction (SAED) patterns of the samples were characterized using a field-emission transmission electron microscope (FE-TEM, JEM-2100 F, JEOL, Japan). The elemental compositions were determined by energy dispersive X-ray spectroscopy (EDS) using the genesis microanalysis system (EDAX) attached to the TEM. Scanning electron microscopy (SEM) images were performed using a Field emission scanning electron microscopy (FESEM, JEOL JSM-7600 F). X-ray photoelectron spectroscopy (XPS) was performed on an X-ray photoelectron spectroscopy (XPS, Thermo Fisher Scientific Theta Probe system). Inductively coupled plasma mass spectrometry (ICP-MS) was analyzed on Optima 7300 DV. BET surface area and pore size measurements were performed with N₂ adsorption/desorption isotherms at 77 K on a Micromeritics ASAP Tri-star II 3020 instrument. Before measurements, the samples were degassed at 150 °C

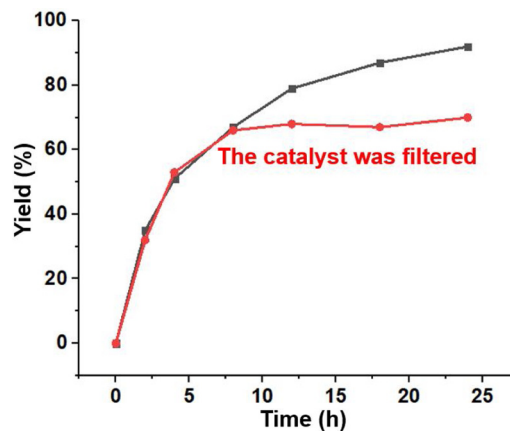
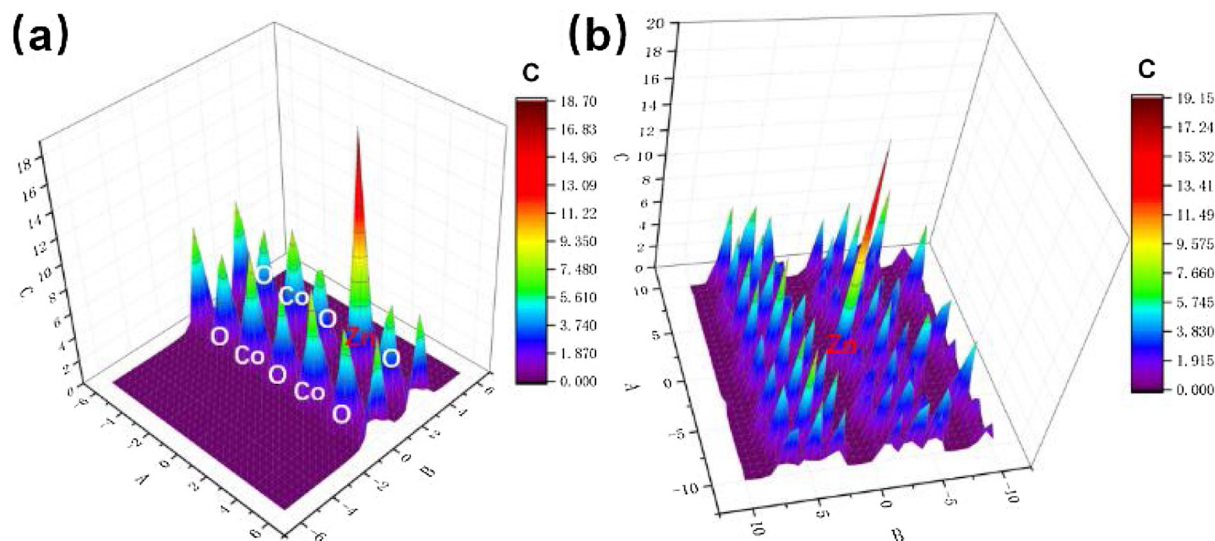


Fig. 10. Hot filtration experiments.

Fig. 9. The charge density maps of (a) CoO-Zn(110) (one Co is replaced by Zn); (b) Co₃O₄-Zn(110) (one Co is replaced by Zn) [56].

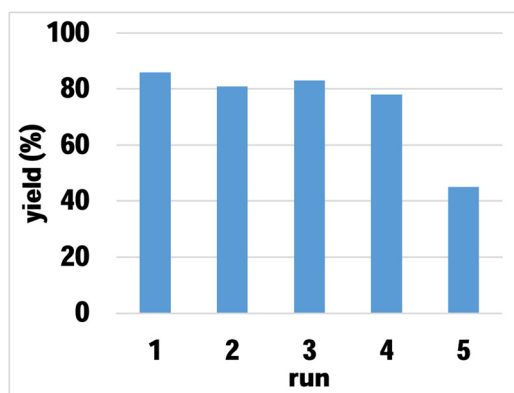


Fig. 11. Recycle studies. Conditions: HMF 3 mmol, Co@CN-Zn12-5 15 mol% of Co, MeOH 3 mL, O₂ 1 atm, 50 °C, 30 h; GC yields with nitrobenzene as an internal standard.

for 12 h. Thermal Gravimetric Analyser (TGA) was detected on a TA Instruments Q500. Temperature-programmed desorption (TPD)-NH₃ and CO₂-TPD were conducted on a Quantachrome TPRWin v3.52 instrument. The samples were pretreated in He flow at 300 °C with a rate of 15 mL/min for 30 min and cooled to 50 °C, and then swept in CO₂ (NH₃) flow with a rate of 15 mL/min for 40 min. After treatment in He flow for 50 min to remove physical adsorption, the sample was raised at a heating rate of 10 °C/min to 800 °C, the signals were monitored by a TCD detector.

The general procedure for the synthesis of Co@CN-ZnX-Y (X for the weight ratio of Zn/Co, Y for the heating rate of pyrolysis)

Chitosan (500 mg), CoCl₂·6H₂O (5 wt.% of Co in chitosan, 100 mg) and Zn(OAc)₂·2H₂O (5X wt.% of Zn in chitosan, 85X mg) were dissolved in a mixture solvent of water and methanol (v/v = 1/1 30 mL). The mixture was stirred at room temperature for 24 h, then continuously stirring at 80 °C for 2 h. Subsequently, the solution was evaporated and transferred into a solid mixture, which was dried at 80 °C for 12 h. The obtained powder was pyrolysis in a tubular furnace under an Ar atmosphere with a heating rate of Y °C/min up to 900 °C for 2 h, followed by cooling to ambient temperature to afford Co@CN-ZnX-Y.

The procedure for the synthesis of Co@AC (active carbon), CoZn@AC, Co@MgO, Co@ZrO₂ and Co@CeO₂

Co@AC (active carbon), Co@MgO, Co@ZrO₂ and Co@CeO₂ were prepared by the typical impregnation method as follows: 1.0 g support (AC, MgO, ZrO₂ and CeO₂) was dispersed into 30 mL aqueous solution of metal precursors (605 mg CoCl₂·6H₂O) under ultrasonic. Lysine aqueous solution (0.53 M) was then added into the mixture with vigorous stirring for 30 min. To this suspension, NaBH₄ aqueous solution (0.05 M) was added dropwise, the mixture was further stirred for 60 min and then aged for 24 h. Finally, the solid was separated, washed (water and ethanol) and dried at room temperature under vacuum. CoZn@AC was synthesized under similar conditions except that the metal precursors were a mixture of CoCl₂·6H₂O (605 mg) and Zn(OAc)₂·2H₂O (56 mg).

The general procedure for the oxidative esterification of HMF

A mixture of HMF (0.3 mmol), Co@CN-ZnX-Y (15 mol% of Co) were added in MeOH (3 mL), which was stirred under 1 atm oxygen at 50 °C for 24 h. After the reaction was completed, the liquid phase was analyzed by GC/MS. The yield of the product was determined by GC with nitrobenzene as an internal standard.

The procedure for the oxidative esterification of HMF in high concentration (1 M)

A mixture of HMF (3 mmol), Co@CN-ZnX-Y (15 mol% of Co) were added in MeOH (3 mL), which was stirred under 1 atm oxygen at 50 °C for 30 h. After the reaction was completed, the liquid phase was analyzed by GC/MS. The yield of the product was determined by GC with nitrobenzene as an internal standard. The recyclability of the Co@CN was investigated under the same reaction conditions (3 mmol HMF in 3 mL of methanol, magnetically stirring, 1 atm oxygen, 50 °C, 30 h) by using the recovered catalysts. After each cycle, the catalyst was isolated from the solution by centrifugation, washed three times with methanol (3 mL × 3), and dried under vacuum to remove the residual solvent and then reused for another reaction cycle.

Declaration of Competing Interest

The authors declare that they have no known competing financial interests or personal relationships that could have appeared to influence the work reported in this paper.

Acknowledgements

We gratefully acknowledge Key Laboratory of Biomass Energy and Material, Jiangsu Province (JSBEM201912), Chinese Postdoctoral Science Foundation (2015M571761, 2016T90465), and A*STAR Science and Engineering Research Council (Grant 1528000048) of the Singapore Government for financial support. This work was a project funded by the Priority Academic Program development of Jiangsu Higher Education Institution.

Appendix A. Supplementary data

Supplementary material related to this article can be found, in the online version, at doi:<https://doi.org/10.1016/j.mcat.2019.110695>.

References

- [1] D.-W. Lee, M.-H. Jin, J.-H. Park, Y.-J. Lee, Y.-C. Choi, Flexible synthetic strategies for lignin-derived hierarchically porous carbon materials, *ACS Synth. Chem. Eng.* 6 (2018) 10454–10462, <https://doi.org/10.1021/acsschemeng.8b01811>.
- [2] X. Kong, Y. Zhu, Z. Fang, J.A. Kozinski, I.S. Butler, L. Xu, H. Song, X. Wei, Catalytic conversion of 5-hydroxymethylfurfural to some value-added derivatives, *Green Chem.* 20 (2018) 3657–3682, <https://doi.org/10.1039/C8GC00234G>.
- [3] Z. Sun, B. Fridrich, A. de Santi, S. Elangovan, K. Barta, Bright side of lignin depolymerization: toward new platform chemicals, *Chem. Rev.* 118 (2018) 614–678, <https://doi.org/10.1021/acs.chemrev.7b00588>.
- [4] K. Wang, J. Jiang, X. Liang, H. Wu, J. Xu, Direct conversion of cellulose to levulinic acid over multifunctional sulfonated humins in sulfolane–water solution, *ACS Sustain. Chem. Eng.* 6 (2018) 15092–15099, <https://doi.org/10.1021/acssuschemeng.8b03558>.
- [5] Z. Zhang, K. Deng, Recent advances in the catalytic synthesis of 2,5-furandicarboxylic acid and its derivatives, *ACS Catal.* 5 (2015) 6529–6544, <https://doi.org/10.1021/acscatal.5b01491>.
- [6] J.J. Bozell, G.R. Petersen, Technology development for the production of biobased products from biorefinery carbohydrates—the US Department of Energy’s “Top 10” revisited, *Green Chem.* 12 (2010) 539–554, <https://doi.org/10.1039/B922014C>.
- [7] F.A. Kucherov, E.G. Gordeev, A.S. Kashin, V.P. Ananikov, Three-dimensional printing with biomass-derived PEF for carbon-neutral manufacturing, *Angew. Chem. Int. Ed.* 56 (2017) 15931–15935, <https://doi.org/10.1002/anie.201708528>.
- [8] A.H. Motagamwala, W. Won, C. Sener, D.M. Alonso, C.T. Maravelias, J.A. Dumesic, Toward biomass-derived renewable plastics: production of 2,5-furandicarboxylic acid from fructose, *Sci. Adv.* 4 (2018) eaap9722, <https://doi.org/10.1126/sciadv.aap9722>.
- [9] D. Yan, J. Xin, Q. Zhao, K. Gao, X. Lu, G. Wang, S. Zhang, Fe–Zr–O catalyzed base-free aerobic oxidation of 5-HMF to 2,5-FDCA as a bio-based polyester monomer, *Catal. Sci. Technol.* 8 (2018) 164–175, <https://doi.org/10.1039/C7CY01704A>.
- [10] S. Xu, P. Zhou, Z. Zhang, C. Yang, B. Zhang, K. Deng, S. Bottle, H. Zhu, Selective oxidation of 5-Hydroxymethylfurfural to 2,5-furandicarboxylic acid using O₂ and a photocatalyst of Co-thioporphyrazine bonded to g-C₃N₄, *J. Am. Chem. Soc.* 139 (2017) 14775–14782, <https://doi.org/10.1021/jacs.7b08861>.
- [11] T. Gao, J. Chen, W. Fang, Q. Cao, W. Su, F. Dumeignil, Ru/Mn Ce1O catalysts with enhanced oxygen mobility and strong metal-support interaction: exceptional performances in 5-hydroxymethylfurfural base-free aerobic oxidation, *J. Catal.* 368

- (2018) 53–68, <https://doi.org/10.1016/j.jcat.2018.09.034>.
- [12] S. Verma, M.N. Nadagouda, R.S. Varma, Porous nitrogen-enriched carbonaceous material from marine waste: chitosan-derived carbon nitride catalyst for aerial oxidation of 5-hydroxymethylfurfural (HMF) to 2,5-furandicarboxylic acid, *Sci. Rep.* 7 (2017) 13596, <https://doi.org/10.1038/s41598-017-14016-5>.
- [13] S. Siankevich, G. Savoglidis, Z. Fei, G. Laurency, D.T.L. Alexander, N. Yan, P.J. Dyson, A novel platinum nanocatalyst for the oxidation of 5-Hydroxymethylfurfural into 2,5-Furandicarboxylic acid under mild conditions, *J. Catal.* 315 (2014) 67–74, <https://doi.org/10.1016/j.jcat.2014.04.011>.
- [14] T. Gao, Y. Yin, W. Fang, Q. Cao, Highly dispersed ruthenium nanoparticles on hydroxyapatite as selective and reusable catalyst for aerobic oxidation of 5-hydroxymethylfurfural to 2,5-furandicarboxylic acid under base-free conditions, *Mol. Catal.* 450 (2018) 55–64, <https://doi.org/10.1016/j.mcat.2018.03.006>.
- [15] B. Sang, J. Li, X. Tian, F. Yuan, Y. Zhu, Selective aerobic oxidation of the 5-hydroxymethylfurfural to 2,5-furandicarboxylic acid over gold nanoparticles supported on graphitized carbon: study on reaction pathways, *Mol. Catal.* 470 (2019) 67–74, <https://doi.org/10.1016/j.mcat.2019.03.026>.
- [16] W.-J. Liu, L. Dang, Z. Xu, H.-Q. Yu, S. Jin, G.W. Huber, Electrochemical oxidation of 5-hydroxymethylfurfural with NiFe layered double hydroxide (LDH) nanosheet catalysts, *ACS Catal.* 8 (2018) 5533–5541, <https://doi.org/10.1021/acscatal.8b01017>.
- [17] D.-H. Nam, B.J. Taitt, K.-S. Choi, Copper-based catalytic anodes to produce 2,5-furandicarboxylic acid, a biomass-derived alternative to terephthalic acid, *ACS Catal.* 8 (2018) 1197–1206, <https://doi.org/10.1021/acscatal.7b03152>.
- [18] M.J. Kang, H. Park, J. Jegal, S.Y. Hwang, Y.S. Kang, H.G. Cha, Electrocatalysis of 5-hydroxymethylfurfural at cobalt based spinel catalysts with filamentous nanoarchitecture in alkaline media, *Appl. Catal. B-Environ.* 242 (2019) 85–91, <https://doi.org/10.1016/j.apcatb.2018.09.087>.
- [19] X.-Y. Zhang, M.-H. Zong, N. Li, Whole-cell biocatalytic selective oxidation of 5-hydroxymethylfurfural to 5-hydroxymethyl-2-furancarboxylic acid, *Green Chem.* 19 (2017) 4544–4551, <https://doi.org/10.1039/C7GC01751K>.
- [20] E. Taarning, I.S. Nielsen, K. Egeblad, R. Madsen, C.H. Christensen, Chemicals from renewables: aerobic oxidation of furfural and hydroxymethylfurfural over gold catalysts, *ChemSusChem* 1 (2008) 75–78, <https://doi.org/10.1002/cssc.200700033>.
- [21] O. Casanova, S. Iborra, A. Corma, Biomass into chemicals: one pot-base free oxidative esterification of 5-hydroxymethyl-2-furfural into 2,5-dimethylfuroate with gold on nanoparticulated ceria, *J. Catal.* 265 (2009) 109–116, <https://doi.org/10.1016/j.jcat.2009.04.019>.
- [22] F. Menegazzo, T. Fantinel, M. Signoretto, F. Pinna, M. Manzoli, On the process for furfural and HMF oxidative esterification over Au/ZrO₂, *J. Catal.* 319 (2014) 61–70, <https://doi.org/10.1016/j.jcat.2014.07.017>.
- [23] F. Menegazzo, M. Signoretto, D. Marchese, F. Pinna, M. Manzoli, Structure–activity relationships of Au/ZrO₂ catalysts for 5-hydroxymethylfurfural oxidative esterification: effects of zirconia sulphation on gold dispersion, position and shape, *J. Catal.* 326 (2015) 1–8, <https://doi.org/10.1016/j.jcat.2015.03.006>.
- [24] F. Li, X.-L. Li, C. Li, J. Shi, Y. Fu, Aerobic oxidative esterification of 5-hydroxymethylfurfural to dimethyl furan-2,5-dicarboxylate by using homogeneous and heterogeneous PdCoBi/C catalysts under atmospheric oxygen, *Green Chem.* 20 (2018) 3050–3058, <https://doi.org/10.1039/C8GC01393D>.
- [25] A. Cho, S. Byun, J.H. Cho, B.M. Kim, AuPd-Fe₃O₄ nanoparticle-catalyzed synthesis of Furan-2,5-dimethylcarboxylate from 5-Hydroxymethylfurfural under mild conditions, *ChemSusChem* 12 (2019) 2310–2317, <https://doi.org/10.1002/cssc.201900454>.
- [26] A. Salazar, P. Hünemörder, J. Rabeah, A. Quade, R.V. Jagadeesh, E. Mejia, Synergistic bimetallic oxidative esterification of 5-hydroxymethylfurfural under mild conditions, *ACS Sustain. Chem. Eng.* 7 (2019) 12061–12068, <https://doi.org/10.1021/acssuschemeng.9b00914>.
- [27] J. Deng, H.J. Song, M.S. Cui, Y.P. Du, Y. Fu, Aerobic oxidation of hydroxymethylfurfural and furfural by using heterogeneous CoxOy-N@C catalysts, *ChemSusChem* 7 (2014) 3334–3340, <https://doi.org/10.1002/cssc.201402843>.
- [28] Y. Sun, H. Ma, X. Jia, J. Ma, Y. Luo, J. Gao, J. Xu, A high-performance base-metal approach for the oxidative esterification of 5-Hydroxymethylfurfural, *ChemCatChem* 8 (2016) 2907–2911, <https://doi.org/10.1002/cctc.201600484>.
- [29] X. Tong, L. Yu, H. Chen, X. Zhuang, S. Liao, H. Cui, Highly efficient and selective oxidation of 5-Hydroxymethylfurfural by molecular oxygen in the presence of Cu-MnO₂ catalyst, *Catal. Commun.* 90 (2017) 91–94, <https://doi.org/10.1016/j.catcom.2016.11.024>.
- [30] K.-k. Sun, S.-j. Chen, Z.-l. Li, G.-p. Lu, C. Cai, Synthesis of a ZIF-derived hollow yolk-shell Co@CN catalyst for the oxidative esterification of 5-hydroxymethylfurfural, *Green Chem.* 21 (2019) 1602–1608, <https://doi.org/10.1039/C8GC03868F>.
- [31] W. Zhong, H. Liu, C. Bai, S. Liao, Y. Li, Base-free oxidation of alcohols to esters at room temperature and atmospheric conditions using nanoscale Co-based catalysts, *ACS Catal.* 5 (2015) 1850–1856, <https://doi.org/10.1021/cs502101c>.
- [32] M.N. Kumar, R.A. Muzzarelli, C. Muzzarelli, H. Sashiwa, A.J. Domb, Chitosan chemistry and pharmaceutical perspectives, *Chem. Rev.* 104 (2004) 6017–6084, <https://doi.org/10.1021/cr030441b>.
- [33] N. Yan, X. Chen, Sustainability: Don't waste seafood waste, *Nature* 524 (2015) 155–157, <https://doi.org/10.1038/524155a>.
- [34] X. Chen, H. Yang, N. Yan, Shell biorefinery: dream or reality? *Chem. Eur. J.* 22 (2016) 13402–13421, <https://doi.org/10.1002/chem.201602389>.
- [35] H. Yang, G. Gözaydin, R.R. Nasaruddin, J.R.G. Har, X. Chen, X. Wang, N. Yan, Toward the shell biorefinery: processing crustacean shell waste using hot water and carbonic acid, *ACS Sustain. Chem. Eng.* 7 (2019) 5532–5542, <https://doi.org/10.1021/acssuschemeng.8b06853>.
- [36] X. Chen, H. Yang, Z. Zhong, N. Yan, Base-catalysed, one-step mechanochemical conversion of chitin and shrimp shells into low molecular weight chitosan, *Green Chem.* 19 (2017) 2783–2792, <https://doi.org/10.1039/c7gc00089h>.
- [37] G. Fu, Z. Cui, Y. Chen, Y. Li, Y. Tang, J.B. Goodenough, Ni₃Fe-N doped carbon sheets as a bifunctional electrocatalyst for air cathodes, *Adv. Energy Mater.* 7 (2017) 1601172, <https://doi.org/10.1002/aenm.201601172>.
- [38] Y. Zhang, L. Lu, S. Zhang, Z. Lv, D. Yang, J. Liu, Y. Chen, X. Tian, H. Jin, W. Song, Biomass chitosan derived cobalt/nitrogen doped carbon nanotubes for the electrocatalytic oxygen reduction reaction, *J. Mater. Chem. A* 6 (2018) 5740–5745, <https://doi.org/10.1039/C7TA11258K>.
- [39] Y. Zhu, W. Sun, W. Chen, T. Cao, Y. Xiong, J. Luo, J. Dong, L. Zheng, J. Zhang, X. Wang, C. Chen, Q. Peng, D. Wang, Y. Li, Scale-up biomass pathway to cobalt single-site catalysts anchored on N-doped porous carbon nanobelt with ultrahigh surface area, *Adv. Funct. Mater.* 28 (2018) 1802167, <https://doi.org/10.1002/adfm.201802167>.
- [40] B. Sahoo, A.-E. Surkus, M.-M. Pohl, J. Radnik, M. Schneider, S. Bachmann, M. Scalone, K. Junge, M. Beller, A Biomass-derived non-noble cobalt catalyst for selective hydrodehalogenation of alkyl and (hetero)aryl halides, *Angew. Chem. Int. Ed.* 56 (2017) 11242–11247, <https://doi.org/10.1002/anie.201702478>.
- [41] Y. Cao, B. Zhao, X. Bao, Y. Wang, Fabricating Metal@N-doped carbon catalysts via a thermal method, *ACS Catal.* 8 (2018) 7077–7085, <https://doi.org/10.1021/acscatal.8b01644>.
- [42] F. Zhang, C. Ma, S. Chen, J. Zhang, Z. Li, X.-M. Zhang, N-doped hierarchical porous carbon anchored tiny Pd NPs: a mild and efficient quinolines selective hydrogenation catalyst, *Mol. Catal.* 452 (2018) 145–153, <https://doi.org/10.1016/j.mcat.2018.04.001>.
- [43] Y. Gao, X. Chen, J. Zhang, N. Yan, Chitin-derived mesoporous, nitrogen-containing carbon for heavy-metal removal and styrene epoxidation, *ChemPlusChem* 80 (2015) 1556–1564, <https://doi.org/10.1002/cplu.201500293>.
- [44] H. Zhong, L. Duan, P. Ye, X. Li, A. Xu, Q. Peng, A. Synthesis of cobalt–nitrogen-doped mesoporous carbon from chitosan and its performance for pollutant degradation as Fenton-like catalysts, *Res. Chem. Intermediat.* 45 (2018) 907–918, <https://doi.org/10.1007/s1164-018-3655-y>.
- [45] Y.Z. Chen, C. Wang, Z.Y. Wu, Y. Xiong, Q. Xu, S.H. Yu, H.L. Jiang, From bimetallic metal-organic framework to porous carbon: high surface area and multicomponent active dopants for excellent electrocatalysis, *Adv. Mater.* 27 (2015) 5010–5016, <https://doi.org/10.1002/adma.201502315>.
- [46] Q. Gu, P. Sautet, C. Michel, Unraveling the role of base and catalyst polarization in alcohol oxidation on Au and Pt in water, *ACS Catal.* 8 (2018) 11716–11721, <https://doi.org/10.1021/acscatal.8b03494>.
- [47] K. Sun, S. Chen, J. Zhang, G.-P. Lu, C. Cai, Cobalt nanoparticles embedded in N-doped porous carbon derived from bimetallic zeolitic imidazolate frameworks for one-pot selective oxidative depolymerization of lignin, *ChemCatChem* 11 (2019) 1264–1271, <https://doi.org/10.1002/cctc.201801752>.
- [48] H. Yang, R. Nie, W. Xia, X. Yu, D. Jin, X. Lu, D. Zhou, Q. Xia, Co embedded within biomass-derived mesoporous N-doped carbon as an acid-resistant and chemoselective catalyst for transfer hydrodeoxygenation of biomass with formic acid, *Green Chem.* 19 (2017) 5714–5722, <https://doi.org/10.1039/C7GC02648J>.
- [49] J.C. Wang, R.F. Nie, L. Xu, X.L. Lyu, X.Y. Lu, Catalytic transfer hydrogenation of oleic acid to octadecanol over magnetic recoverable cobalt catalysts, *Green Chem.* 21 (2019) 314–320, <https://doi.org/10.1039/C8GC03075H>.
- [50] B. Liu, L. Jin, H. Zheng, H. Yao, Y. Wu, A. Lopes, J. He, Ultrathin Co-based nanoparticle@mesoporous carbon nanospheres toward high-performance supercapacitors, *ACS Appl. Mater. Interfaces* 9 (2017) 1746–1758, <https://doi.org/10.1021/acsami.6b11958>.
- [51] B. An, J. Zhang, K. Cheng, P. Ji, C. Wang, W. Lin, Confinement of ultrasmall Cu/ZnOx nanoparticles in metal-organic frameworks for selective methanol synthesis from catalytic hydrogenation of CO₂, *J. Am. Chem. Soc.* 139 (2017) 3834–3840, <https://doi.org/10.1021/jacs.7b00058>.
- [52] K. Vankudoth, A.H. Padmasri, R. Sarkari, V.K. Velisoju, N. Gutta, N.K. Sathu, C.N. Rohita, V. Akula, The role of Lewis acid–base pair sites in ZnO-ZnCr₂O₄ catalysts for cyclization via dehydrogenative condensation of crude glycerol and 1,2-propanediamine for the synthesis of 2,6-dimethylpyrazine, *New J. Chem.* 41 (2017) 9875–9883, <https://doi.org/10.1039/C7NJ01819C>.
- [53] W.R. Leow, W.K.H. Ng, T. Peng, X. Liu, B. Li, W. Shi, Y. Lum, X. Wang, X. Lang, S. Li, N. Mathews, J.W. Ager, T.C. Sum, H. Hirao, X. Chen, Al₂O₃ surface complexation for photocatalytic organic transformations, *J. Am. Chem. Soc.* 139 (2017) 269–276, <https://doi.org/10.1021/jacs.6b09934>.
- [54] E. Hayashi, Y. Yamaguchi, K. Kamata, N. Tsunoda, Y. Kumagai, F. Oba, M. Hara, Effect of MnO₂ crystal structure on aerobic oxidation of 5-hydroxymethylfurfural to 2,5-furandicarboxylic acid, *J. Am. Chem. Soc.* 141 (2019) 890–900, <https://doi.org/10.1021/jacs.8b09917>.
- [55] H. Su, K.-X. Zhang, B. Zhang, H.-H. Wang, Q.-Y. Yu, X.-H. Li, M. Antonietti, J.-S. Chen, Activating cobalt nanoparticles via the Mott–Schottky effect in nitrogen-rich carbon shells for base-free aerobic oxidation of alcohols to esters, *J. Am. Chem. Soc.* 139 (2017) 811–818, <https://doi.org/10.1021/jacs.6b10710>.
- [56] L.N. Kantorovich, User-Friendly Visualisation Program for Ab Initio DFT Codes VASP and SIESTA, (2019), pp. 1996–2007.